RESEARCH ARTICLE

Electrospinning polyethylene terephthalate glycol

Mohamed H. Hassan[1]*, Abdalla M. Omar[1], Evangelos Daskalakis[1], Bruce Grieve[2], and Paulo J.D.S. Bartolo[1,3]

[1]Department of Mechanical, Aerospace and Civil Engineering, University of Manchester, Manchester, M13 9PL, United Kingdom

[2]Department of Electrical and Electronic Engineering, The University of Manchester, Manchester M13 9PL, United Kingdom

[3]Singapore Centre for 3D Printing, School of Mechanical and Aerospace Engineering, Nanyang Technological University, Singapore 639798, Singapore

Abstract

Polyethylene terephthalate glycol (PETG) is a difficult-to-spin material, and no previous papers have reported the correct conditions to create PETG meshes. To address this issue, a preliminary study on the solubility and electrospinnability of PETG using a range of solvent system was conducted and a Teas graph was established to select the ideal solvent system. Based on these preliminary results, electrospun PETG fibers were produced using a highly volatile binary solvent system consisting of dichloromethane (DCM) and trifluoroacetic acid (TFA). Produced meshes were extensively characterized, and the results demonstrated for the first time the ability of electrospun PETG meshes to support the inoculation and germination of yellow rust spores, thus confirming that PETG is an ideal material to be used for the fabrication of agriculture biosensors. The results also showed that the best solvent split was 85/15 (DCM/TFA).

Keywords: Electrospinning; Biomaterial; Yellow rust; Polyethylene terephthalate glycol; bioactive

1. Introduction

Solution electrospinning is a simple electrostatic and versatile technique to produce micro- to nano-scale fiber meshes exhibiting large surface area to volume ratio[1-4]. In this process, a polymeric solution is ejected from a needle tip, positioned at a specific height over a grounded collector, by applying a high electrical field[5]. Typically, an electrospinning system consists of a high-voltage power supply, a capillary that includes the material container and a spinneret, and a grounded metal collector. The process starts by applying an electrical field between the needle tip and the metallic collector. A material droplet is formed at the end of the needle tip because of surface tension and viscoelastic stresses[6]. When the electrostatic forces overcome the surface tension of the material, the material droplet approaches a cone shape (Taylor cone), and a charged jet is ejected[7]. Then, the jet follows a path that is usually characterized by an initial stable region, where the fiber is parallel to the direction of the jet and its

diameter decreases monotonically by increasing the distance from the tip[5]. Afterward, the jet starts to coil and undergo bending instabilities that further reduces the fiber diameter. Fibers produced by electrospinning presents a large control over the fiber diameters, ranging from nano- to micro-meters[8,9]. These fibers compared to microfibers produced by other conventional spinning techniques, including melt spinning, dry spinning, and wet spinning, have significantly reduced diameters, thus increasing the specific surface area of the produced structures[10,11]. These distinctive features led to electrospinning being used for a range of applications such as support structures for cell attachment, proliferation, and differentiation[5,6,12,13], wound dressings[14,15], and sensing membranes[16,17]. Electrospinning was reported to be a viable technique for the encapsulation of cells, thus allowing the fabrication of cell-laden structures[18,19]. Modular systems, combining solution electrospinning and other additive manufacturing techniques such as extrusion, have been also proposed for the fabrication of hierarchical constructs[4,20,21]. In this work, electrospinning is investigated as a potential technology to produce the upper layer of the proposed biosensor for the early detection of yellow rust. The proposed biosensor consists of three layers, where the first layer imitates the morphology of wheat leaf, the second layer is the substrate layer where sucrose and agar are used as a feeding media for the germinate spore, and finally the third layer is made up of a nonenzymatic glucose sensor which is used to detect the glucose produced by the interaction between the invertase produced by the germinated spores and the substrate layer[22]. As electrospinning allows to produce meshes with high surface area, this will increase the capability to support pathogen inoculation and germination.

In previous work, it was also shown that polyethylene terephthalate glycol (PETG) is an ideal material for the fabrication of the upper layer due to its shape changing properties, biodegradability, and ability to support cell attachment and proliferation, suggesting a similar behavior regarding the yellow rust[23,24]. However, PETG has low solubility in most solvents, which are also usually highly volatile, making it difficult for electrospinning.

In this study, we investigated for the first-time the fabrication of electrospun PETG meshes. A preliminary study on the solubility and electrospinnability of PETG using a range of solvent systems was conducted, and a Teas graph was established to select the ideal solvent system. Based on these preliminary results, electrospun PETG fibers were produced and extensively characterized. The results also demonstrated for the first time the ability of electrospun PETG meshes to support the inoculation and germination of yellow rust spores, thus confirming that PETG is an ideal material to be used in the proposed

biosensor. *Puccinia striiformis* f. sp. *tritici* is a causative fungal pathogen that causes wheat yellow rust, which is currently a global epidemic responsible for reduction in the wheat yield. Using sensing systems to detect such diseases can help in taking preventative actions to reduce its effect.

In this work, we also investigated for the first-time producing PETG meshes via electrospinning, investigated effects of different solvent splits on meshes quality, and optimized the electrospinning process parameters. Electrospinning is used as a proof of concept for future production of PETG meshes using more advanced techniques such as electrohydrodynamic printing (EHDP)[25]. Furthermore, the meshes bioactivity was assessed by growing yellow rust spores to prove the concept of usage in sensing systems.

2. Materials and methods

2.1. Materials

Polymeric electrospun meshes were produced using PETG with molecular weight of 300 g/mol purchased from RS components (Northants, UK). Solutions were prepared using acetic acid (AA; glacial, ACS reagent ≥99.7%), acetone (ACE; ACS reagent ≥99.5%), ethanol (ETH; 98%), dimethyl sulfoxide (DMSO; ACS reagent ≥99.9%), dimethylformamide (DMF; ACS reagent ≥99.8%), tetrahydrofuran (THF; ACS reagent ≥99.0%), dichloromethane (DCM; containing 40-150 ppm amylene as stabilizer, ACS reagent, ≥99.5%), and trifluoroacetic acid (TFA; 99%), which were all purchased from Sigma Aldrich (Dorset, UK).

2.2. Mapping spinnability–solubility of PETG on the Teas graph

The solubility of PETG in the different solvents was investigated using the Teas graph to identify the fractional cohesion parameters of solvents (hydrogen bonding, polar force, and dispersion force)[26-29]. Solubility was tested at 20% w/v polymer concentration, atmospheric pressure, and room temperature (20°C). Briefly, 2 g of PETG were added to 10 mL of single solvent systems (AA, ACE, ETH, DMSO, DMF, THF, DCM, or TFA) and binary solvent systems (DCM/DMF, DCM/AA, DCM/THF, or DCM/TFA). The mixture was stirred with a magnetic stirring bar at room temperature. The process was visually assessed after 1 h, 2 h, and 4 h. Then, solubilities were categorized as insoluble (no dissolution), partially soluble (dissolution achieved but at lower rate or lower capacity), and soluble (quick and complete dissolution), based on the time to form a homogeneous solution. The binary solvent systems were also identified and calculated using the lever rule assuming 1:1 ratio[30]. Finally, the solubility results of the binary solvent systems were compared to the single solvent
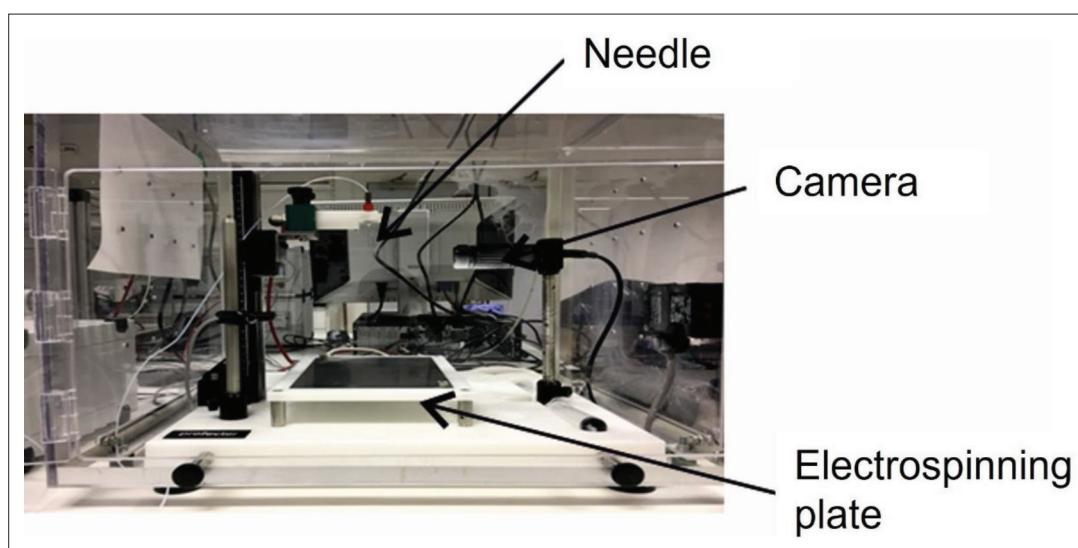
Figure 1. Electrospinning setup

systems on the Teas graph, and then the solubility region was constructed.

2.3. Mesh fabrication

Based on the solubility results, PETG (20% w/v) was dissolved in different splits of DCM/TFA (85/15, 70/30, 60/40, 50/50, 40/60, 30/70, 15/85 [% v/v]), and electrospun using solution electrospinning (Spraybase, Ireland) (Figure 1). Meshes were produced at room temperature with a voltage of 16 kV, a feed flow rate of 4 mL/h, a humidity of 45% (±5%), and a distance between the needle tip and the collector, which was covered with aluminum foil, of 150 mm. Finally, the obtained meshes were dried in vacuum for 48 hours to ensure the complete removal of solvents. These were considered the optimized parameters. Voltage values lower than 16 kV did not enable the formation of a stable jet but only caused a dropping effect, while values higher than 16 KV induced electrospraying. Moreover, flow rate values lower than 4 mL/h induced a fast evaporation of the solvent blocking the needle, while values above 4 mL/h caused a dropping effect.

2.4. Morphological analysis

The morphology of produced meshes was characterized using the scanning electron microscopy (SEM). For SEM, Quanta 650 (FEI company, Hillsboro, Oregon, USA) was used, all meshes were sputter coated with gold/palladium (Au/Pd (80/20)) using Quorum sputter coater (Quorum tech, east Sussex, UK). Imaging was carried out using an acceleration voltage of 15 kV. The obtained images were analyzed using the ImageJ software (Laboratory for Optical and Computational Instrumentation, University of Wisconsin, WI, USA), allowing to determine fiber diameter. For each mesh type, a total of 9 measurements were considered.

2.5. Chemical composition characterization

The chemical composition of produced meshes was analyzed using Fourier-transform infrared spectroscopy (FTIR) and Raman spectroscopy. FTIR was conducted using Varian 670-IR spectrometer (Agilent Technologies, CA, USA). Each sample was scanned 20 times at the resolution of 1 cm^{-1}, over a frequency scanning range from 800 to 3100 cm^{-1}. Raman spectroscopy was carried out using Renishaw inVia confocal Raman microscope (Renishaw Plc., Gloucestershire, UK) using laser (532 nm) with a grating of 1200 g/mm in a regular mode and use of 50× magnification on the microscope.

2.6. Inoculation

The ability of the electrospun meshes to sustain pathogen attachment and germination was assessed using the yellow rust spores' inoculation process. The meshes were placed in a tray in a stainless-steel pipe, simulating a wind tunnel. The spores were released in the pipe, landing on the meshes at the bottom of the pipe. The meshes were kept in the pipe for 15–30 min, ensuring that all spores have settled on the surfaces. Then, the inoculated surfaces were imaged under a light microscope to make sure that the spores were attached. Finally, the meshes were placed in the Innova 44 incubator (Eppendorf, Hamburg, Germany) set at 7°C for 24 h.

3. Results and discussion

3.1. Solubility and electrospinnability

Solubility, which describes how easy it is to dissolve the polymer in a solvent, and electrospinnability,
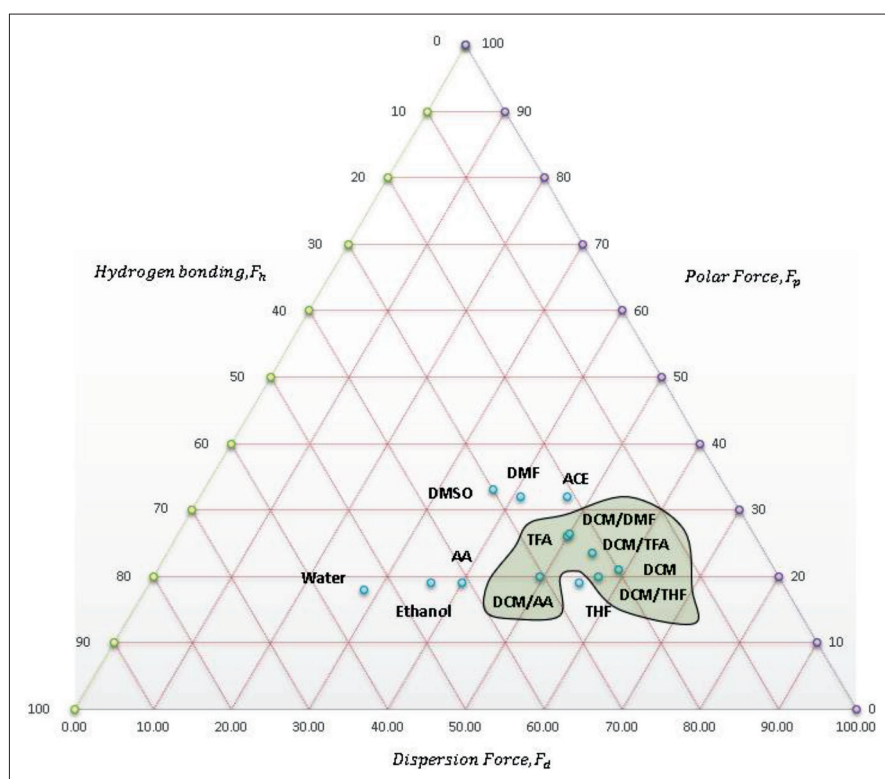
Figure 2. Solubility–spinnability map of PETG based on the Teas graph. The contoured region presents the solvents that can dissolve PETG into a homogenous solution.

which describes the ability of a polymeric solution to be stretched under a specific current, were investigated for different solvents, and the results are presented in Figure 2. The lower right quadrant in Figure 2 presents the best solutions for the dissolution of PETG in TFA or DCM. These solvents can produce nanofibers as single and binary solvent systems. As DCM showed the highest solubility, we decided to investigate its use combined with other solvents (binary solvent systems) such as DCM/DMF, DCM/AA, DCM/THF, and DCM/TFA. The results showed that the DCM/TFA binary solvent system allowed the best spinnability. Therefore, the effect of different splits of DCM/TFA on meshes production was investigated.

However, there were some challenges regarding the reproducibility of the meshes and stability of the Taylor cone due to the high evaporation rate of the solvents. Two parameters were investigated to address this issue. First, a high flow rate was used to stabilize the Taylor cone and counteract the rapid evaporation rate of the binary solvent system. Second, based on a preliminary investigation on the effect of the relative humidity on the spinnability, relative humidity was fixed at around 45% (±5%) allowing the best spinnability condition as the evaporation rate of the solvent would be limited.

3.2. Morphology

Figure 3 presents SEM images at 1000× magnification of the produced meshes. As seen from Figure 3A–G, the fiber thickness and porosity decreases by increasing the content of TFA (more viscous than DCM), while fiber roughness and bead content increases. Moreover, as DCM is a stronger solvent (higher polar force) but has a slower evaporation rate, it contributes to the formation of fibers with higher thickness. Therefore, by controlling the ratio between DCM and TFA, it is possible to control the thickness, roughness, and porosity of the fibers, thus allowing to create meshes with different fiber densities. In this study, the optimal mesh density, as shown in Figure 3D, is based on a 50/50 (% v/v) DCM/TFA system. This mesh exhibits optimal morphology by presenting thin fibers, lower porosities, and absence of beads.

Moreover, meshes produced from 85/15, 70/30, 60/40, 50/50 (% v/v) solutions were bead-free, while meshes produced from 40/60, 30/70, 15/85 (% v/v) solutions had beads.

Table 1 presents average fiber diameter per mesh. The average fiber diameter decreases proportionally with the decrease of DCM. This can be attributed to the volatility
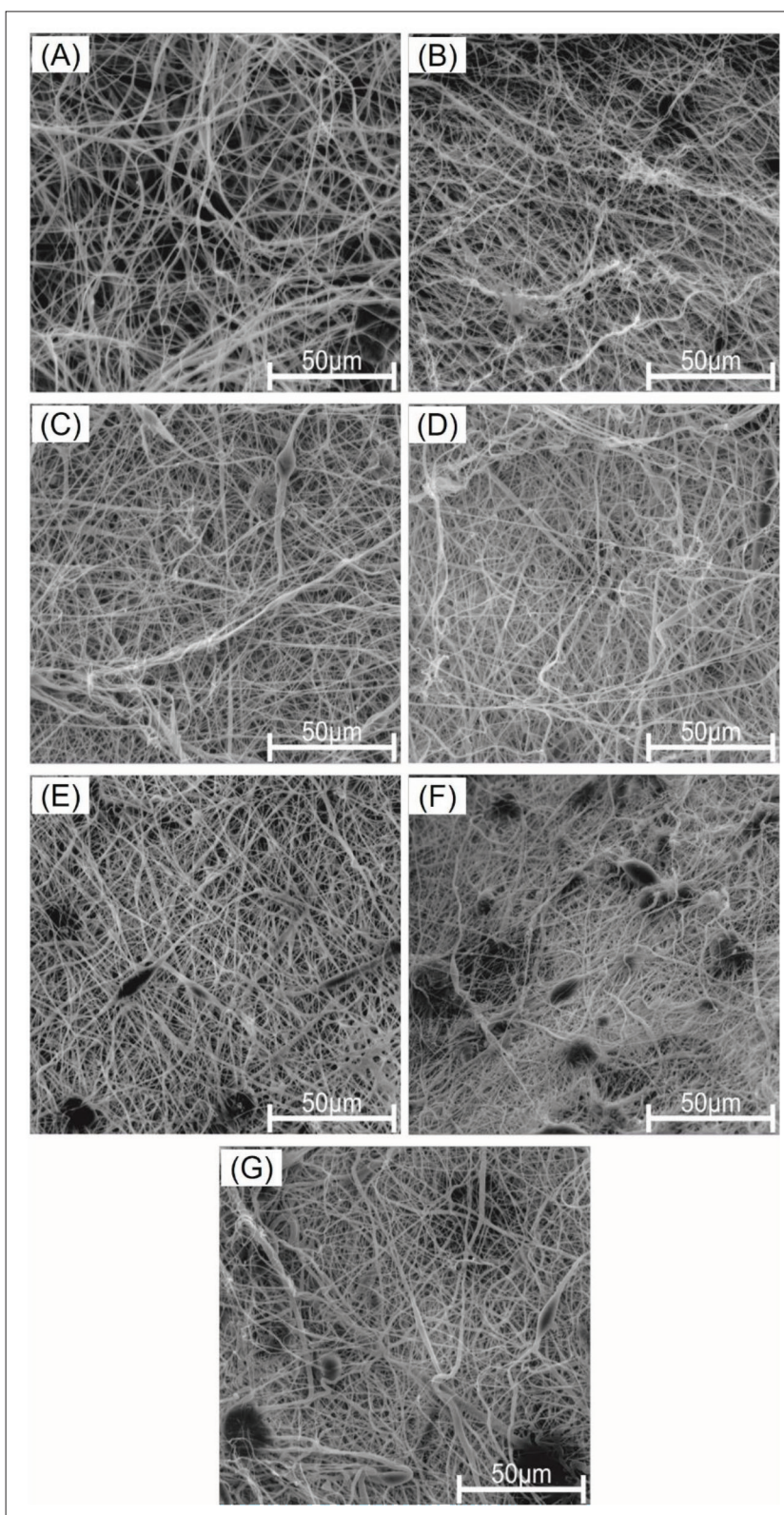
Figure 3. SEM image of the electrospun PETG using different solvent splits (DCM/TFA) with 1000× magnification. (A) 85/15, (B) 70/30, (C) 60/40, (D) 50/50, (E) 40/60, (F) 30/70, and (G) 15/85.

Table 1. Average fiber diameter based on the solvent split

Solution (DCM/TFA) (% v/v)	Fiber diameter (μm)
85/15	1.108 ± 0.181
70/30	0.800 ± 0.1307
60/40	0.677 ± 0.221
50/50	0.559 ± 0.162
40/60	0.428 ± 0.084
30/70	0.289 ± 0.079
15/85	0.243 ± 0.100

of the solvents, as TFA is more volatile than DCM, which causes rapid evaporation that leads to thinner fibers.

3.3. Mesh composition

The chemical composition of the electrospun PETG meshes was investigated using FTIR, a non-destructive analytical technique that allows to qualitatively assess the crystallinity of the electrospun meshes. Figure 4 shows the FTIR spectra for the different electrospun meshes. Common PETG characteristic peaks were recorded at 965 cm^{-1} (C–H stretching peak of cyclohexylene ring)[31], 1106 cm^{-1} (in-plane vibrations of the C–H bonds)[31], 1260 cm^{-1} (ester groups)[31], 1717 cm^{-1} (C=O ester group)[31], 2861 cm^{-1} and 2939 cm^{-1} (C–H symmetrical and asymmetrical stretching vibration in the aliphatic polymeric chains)[31].

As the C–H stretching of cyclohexene ring increases, it can be concluded that the cyclohexanedimethanol (CHDM; amorphous material) content also increases and crystallinity decreases[23]. Moreover, from the different solvent splits, it can be noted that the TFA dominant splits have a slightly higher crystallinity compared to DCM dominant splits.

Raman spectroscopy was used as a non-destructive, robust, and rapid analytical technique to qualitatively assess the chemical difference between different electrospun meshes. The results are presented in Figure 5. All obtained spectra were treated with baseline correction by subtracting a polynomial fit of the baseline from the raw spectra. This was done to remove the tilted baseline variation occurring due to different noises.

Common PETG characteristic peaks were obtained at 793 cm^{-1} (C–H ring out-of-plane bending + C = O bending)[32], 900 cm^{-1} (C–H ring out-of-plane-bending)[32], 1021 cm^{-1} (C–H ring in-plane bending)[32], 1116 cm^{-1} (C–O stretching)[32], 1273 cm^{-1} (C–O stretching of ester group)[32], 1377 cm^{-1} (gauche CH_2 wagging)[32], 1502 cm^{-1} (—CH_2 bending peak of the PETG macromolecular chain backbone)[32], 1613 cm^{-1} (symmetric stretching of the 1,4 para di-substituted benzene ring)[33], and 1727 cm^{-1} (C = O stretching of ester group)[32].

The crystallinity of PETG can be seen from the 1116 cm^{-1} (C–O stretching) as it is slightly shifted to the right and exhibits shoulder band at ~1190 cm^{-1}. In addition, the peak at 1727 cm^{-1} appears wider for lower crystalline materials. Both phenomena were observed in DCM dominant solvent splits, which were lower in crystallinity[34].

3.4. Inoculation

The bioactivity of produced meshes was assessed using spore inoculation. After inoculating the meshes with yellow rust spores, they were placed in the incubator for 24 h. The meshes were then removed from the incubator and inspected to assess its bioactivity. Figure 6A presents the SEM image at 0 h where the spores are shown to be dispersed on the meshes. Figure 6B shows the clusters growth of the fungal spores after 24 h. Figure 6C and D present magnified images of the germinated germ tubes, proving the bioactivity of the produced meshes that encourages the growth of fungal spores. This proves that the produced meshes are bioactive, enabling the growth of the fungal spores.

4. Conclusion

In this study, we investigated strategies to create PETG electrospinning meshes, a polymeric material that is difficult to spin. To the best of our knowledge, this was the first attempt to create PETG meshes using solution electrospinning. Multiple single and binary solvent systems were used to investigate the solubility of PETG, and it was found that DCM/TFA presented the best solubility–spinnability results among the different solvents. Optimal processing conditions were determined, and final meshes were produced at a flow rate of 4 mm/h, a voltage of 16 kV, and a humidity of 40%–50%. Meshes obtained under optimal processing conditions were chemically characterized using both FTIR and Raman spectroscopy, and the results showed that meshes produced using DCM dominant splits have lower crystallinity, where meshes produced using TFA dominant splits have higher crystallinity. This can be attributed to the difference in volatility and evaporation rate of DCM and TFA. Morphological characterization was performed using SEM and the results showed the presence of beads in TFA dominant splits, whereas DCM dominant splits were bead-free. Moreover, meshes produced using DCM/TFA (1:1) presents the best trade-off between fiber thickness and surface roughness. Inoculation on the optimal mesh was carried, to investigate the bioactivity, and the results demonstrated fungal germination and proliferation of the yellow rust spores on these meshes. Our results suggest that the produced electrospun PETG meshes have high potential to be used in sensing applications.
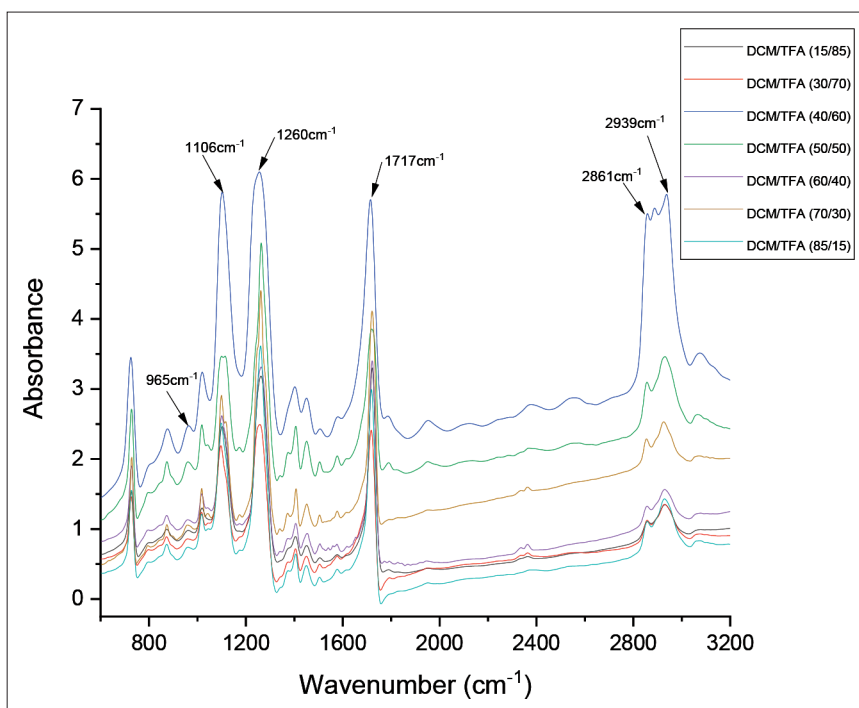
Figure 4. FTIR spectra of electrospun PETG using different solvent splits (DCM/TFA).
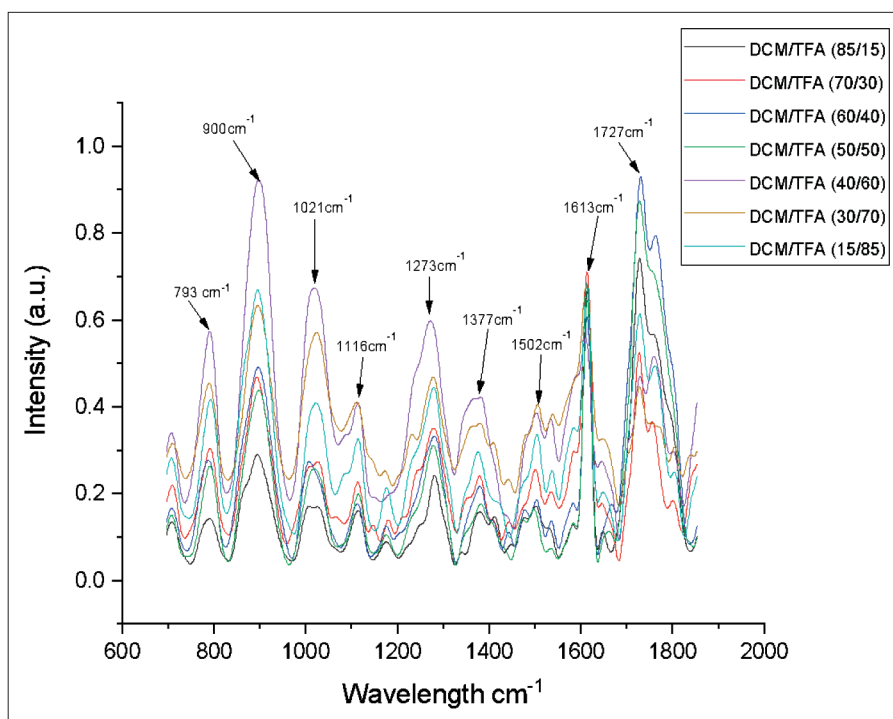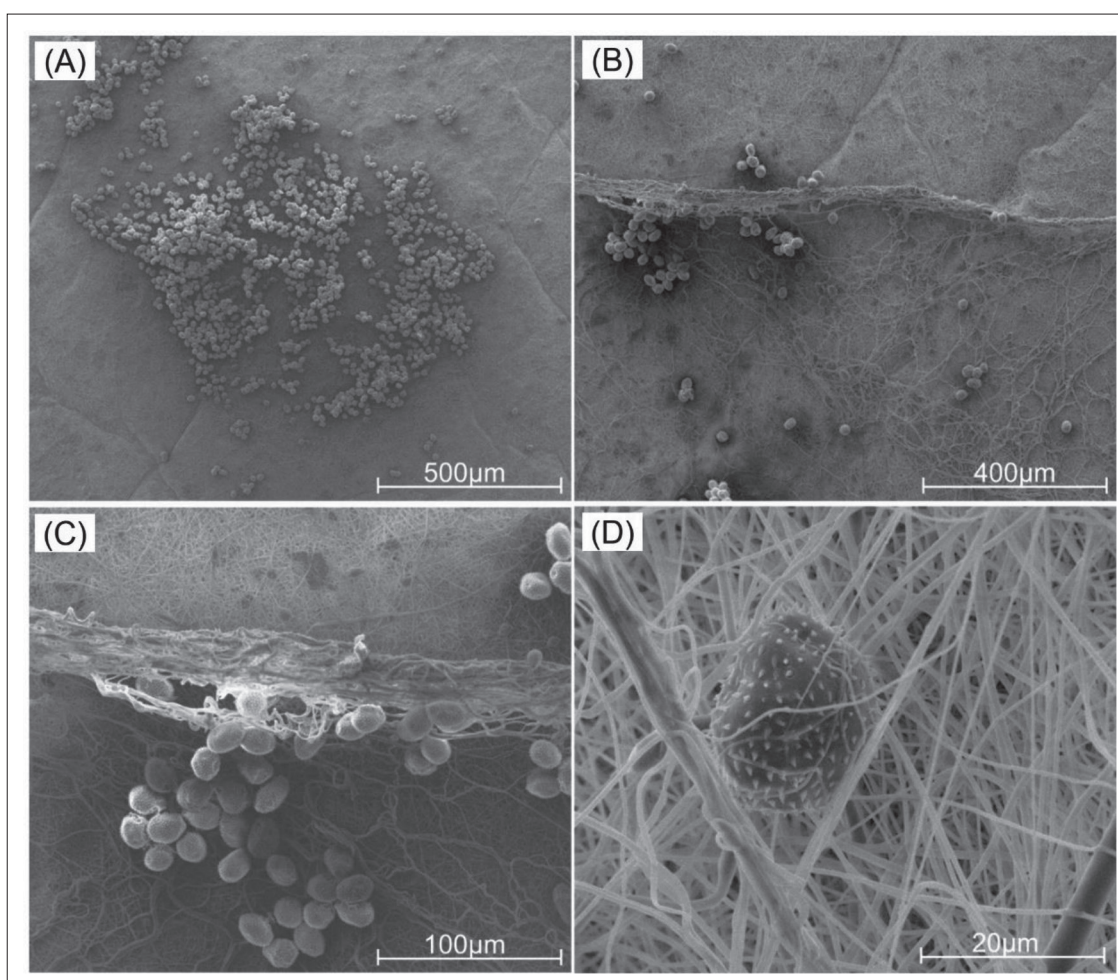

Figure 5. RAMAN spectra of electrospun PETG using different solvent splits (DCM/TFA).

Figure 6. (A) SEM image of *P. striiformis* f. sp. *tritici* spores (100× magnification) at 0 h of inoculation. (B) SEM image of *P. striiformis* f. sp. *tritici* spores (200× magnification) after 24 h. (C) SEM image of the germinated *P. striiformis* f. sp. *tritici* spores (500× magnification). (D) SEM image of the germinated *P. striiformis* f. sp. *tritici* spores (2000× magnification).

Acknowledgments

Conflict of interest

The authors declare no conflict of interest.

Author contributions

Conceptualization: Mohamed H. Hassan
Data curation: All authors
Formal analysis: Mohamed H. Hassan, Abdalla M. Omar, Evangelos Daskalakis
Funding acquisition: Paulo J.D.S. Bartolo
Investigation: Mohamed H. Hassan, Abdalla M. Omar, Evangelos Daskalakis
Methodology: Mohamed H. Hassan, Abdalla M. Omar, Evangelos Daskalakis
Project administration: Paulo J.D.S. Bartolo, Bruce Grieve
Resources: All authors
Software: Mohamed H. Hassan, Abdalla M. Omar, Evangelos Daskalakis
Supervision: Paulo J.D.S. Bartolo, Bruce Grieve
Validation: Mohamed H. Hassan, Abdalla M. Omar, Evangelos Daskalakis
Visualization: All authors
Writing – original draft: All authors
Writing – review and editing: All authors

All authors have read and agreed to the published version of the manuscript.

References

1. Mota C, Puppi D, Dinucci D, *et al.*, 2011, Dual-scale polymeric constructs as scaffolds for tissue engineering. *Materials*, 4(3): 527–542.

2. Dias JR, Sousa A, Augusto A, *et al.*, 2022, Electrospun polycaprolactone (PCL) degradation: An in vitro and in vivo study. *Polymers*, 14(16): 3397.

3. Aslan E, Vyas C, Yupanqui MJ, *et al.*, 2011, Preliminary characterization of a polycaprolactone-SurgihoneyRO electrospun mesh for skin tissue engineering. *Materials*, 15(1): 89.

4. Huang B, Aslan E, Jiang Z, *et al.*, 2020, Engineered dual-scale poly (ε-caprolactone) scaffolds using 3D printing and rotational electrospinning for bone tissue regeneration. *Addit Manuf*, 36: 101452.

5. Motamedi AS, Mirzadeh H, Hajiesmaeilbaigi F, *et al.*, 2017, Effect of electrospinning parameters on morphological properties of PVDF nanofibrous scaffolds. *Progr Biomater*, 6: 113–123.

6. Mei Q, Fu R, Ding Y, *et al.*, 2019, Electrospinning of highly dispersed Ni/CoO carbon nanofiber and its application in glucose electrochemical sensor. *J Electroanalyt Chem*, 847: 113075 %@ 1572–6657.

7. Yarin AL, Koombhongse S, Reneker DH, 2001, Taylor cone and jetting from liquid droplets in electrospinning of nanofibers. *J Appl Phys*, 90(9): 4836–4846.

8. Wu S, Liu J, Qi Y, *et al.*, 2021, Tendon-bioinspired wavy nanofibrous scaffolds provide tunable anisotropy and promote tenogenesis for tendon tissue engineering. *Mater Sci Eng C*, 126: 112181.

9. Li Y, Wang J, Qian D, *et al.*, 2021, Electrospun fibrous sponge via short fiber for mimicking 3D ECM. *J Nanobiotechnol*, 19(1): 131.

10. Li M, Qiu W, Wang Q, *et al.*, 2022, Nitric oxide-releasing tryptophan-based poly (ester urea) s electrospun composite nanofiber mats with antibacterial and antibiofilm activities for infected wound healing. *ACS Appl Mater Interfaces*, 14(14): 15911–15926.

11. Qi Y, Wang C, Wang Q, *et al.*, 2023, A simple, quick, and cost-effective strategy to fabricate polycaprolactone/silk fibroin nanofiber yarns for biotextile-based tissue scaffold application. *Eur Polym J*, 186: 111863.

12. Vyas C, Ates G, Aslan E, *et al.*, 2020, Three-dimensional printing and electrospinning dual-scale polycaprolactone scaffolds with low-density and oriented fibers to promote cell alignment. *3D Print Addit Manuf*, 7(3): 105–113.

13. Hunley MT, Long TE, 2008, Electrospinning functional nanoscale fibers: A perspective for the future. *Polym Int*, 57(3): 385–389.

14. Tang Y, Lan X, Liang C, *et al.*, 2019, Honey loaded alginate/PVA nanofibrous membrane as potential bioactive wound dressing. *Carbohydr Polym*, 219: 113–120.

15. Stojkovska J, Djurdjevic Z, Jancic I, *et al.*, 2018, Comparative in vivo evaluation of novel formulations based on alginate and silver nanoparticles for wound treatments. *J Biomater Appl*, 32(9): 1197–1211.

16. Yang X, Wang Y, Qing X, 2019, A flexible capacitive sensor based on the electrospun PVDF nanofiber membrane with carbon nanotubes. *Sens Actuators A Phys*, 299: 111579.

17. Hussain Z, Ullah S, Yan J, *et al.*, 2022, Electrospun tannin-rich nanofibrous solid-state membrane for wastewater environmental monitoring and remediation. *Chemosphere*, 307: 135810.

18. Townsend-Nicholson A, Jayasinghe SN, 2006, Cell electrospinning: A unique biotechnique for encapsulating living organisms for generating active biological microthreads/scaffolds. *Biomacromolecules*, 7(12): 3364–3369.

19. Hong J, Yeo M, Yang GH, *et al.*, 2019, Cell-electrospinning and its application for tissue engineering. *Int J Mol Sci*, 20(24): 6208.

20. Liu F, Vyas C, Poologasundarampillai G, *et al.*, 2018, Structural evolution of PCL during melt extrusion 3D printing. *Macromol Mater Eng*, 303(2): 1700494.

21. Bartolo P, Malshe A, Ferraris E, *et al.*, 2022, 3D bioprinting: Materials, processes, and applications. *CIRP Ann*, 71(2): 577–597.

22. Hassan MH, Omar AM, Daskalakis E, *et al.*, 2022, Multi-layer biosensor for pre-symptomatic detection of *Puccinia strifformis*, the causal agent of yellow rust. *Biosensors*, 12(10): 829.

23. Hassan MH, Omar AM, Daskalakis E, *et al.*, 2020, Preliminary studies on the suitability of PETG for 4D printing applications, in *7th International Conference of Materials and Manufacturing Engineering (ICMMEN 2020)*, 6.

24. Hassan MH, Omar AM, E. Daskalakis, *et al.*, 2020, The potential of polyethylene terephthalate glycol as biomaterial for bone tissue engineering. *Polymers*, 12(12): 3045.

25. Paralı L, Koç M, Yıldız Z, 2022, 2D/3D direct writing of thermoplastics through electrohydrodynamic printing. *Polym Sci Series A*, 64(5): 559–572.

26. Luo C, Nangrejo M, Edirisinghe M, 2010, A novel method of selecting solvents for polymer electrospinning. *Polymer*, 51(7): 1654–1662.

27. Barton AF, 2017, *CRC Handbook of Solubility Parameters and Other Cohesion Parameters*, Routledge.

28. Heseltine PL, Ahmed J, Edirisinghe M, 2018, Developments in pressurized gyration for the mass production of polymeric fibers. *Macromol Mater Eng*, 303(9): 1800218.

29. Luo C, Stride E, Edirisinghe M, 2012, Mapping the influence of solubility and dielectric constant on electrospinning polycaprolactone solutions. *Macromolecules*, 45(11): 4669–4680.

30. Burke J, 1984, *Solubility Parameters: Theory and Application.* The AIC book and paper group annual, 3: 13–58.

31. Paszkiewicz S, Szymczyk A, Pawlikowska D, *et al.*, 2017, Synthesis and characterization of poly (ethylene terephthalate-co-1, 4-cyclohexanedimethylene terephtlatate)-block-poly (tetramethylene oxide) copolymers. *RSC Adv*, 7(66): 41745–41754.

32. Cole K, Guevremont J, Ajji A, *et al.*, 1994, Characterization of surface orientation in poly (ethylene terephthalate) by front-surface reflection infrared spectroscopy. *Appl Spectrosc*, 48(12): 1513–1521.

33. Alexiou VF, Mathioudakis GN, Andrikopoulos KS, *et al.*, 2020, Poly (ethylene terephthalate) carbon-based nanocomposites: A crystallization and molecular orientation study. *Polymers*, 12(11): 2626.

34. Ciera L, Beladjal L, Almeras X, *et al.*, 2014, Morphological and material properties of polyethyleneterephthalate (PET) fibres with spores incorporated. *Fibres Text East Eur,* 22(4): 29–36.